*Int. J. Electrochem. Sci.*, 9 **(2014)** 1902 - 1910

International Journal of
ELECTROCHEMICAL
SCIENCE
www.electrochemsci.org

*Short Communication*

# Numerical Simulation of Heat/Mass Transfer in a Single Proton Exchange Membrane Fuel Cell with Serpentine Fluid Channels

*HU Guilin*[*], *Yousheng Xu, Zhiguo Zhang*

School of Light Industry, Zhejiang University of Science and Technology, Hangzhou, 310023, P. R. China
[*]E-mail: enehgl@163.com

*Received:* 19 November 2013 / *Accepted:* 30 December 2013 / *Published:* 2 February 2014

The proton exchange membrane fuel cell (PEMFC) has become the promising candidate for power source of electrical vehicle for its advantage characteristics as no pollution, low noise and especially fast startup under common temperature. A three-dimensional, non-isothermal and two-phase mathematical model based on computation fluid dynamics is developed to describe flow and heat transfer process of a PEMFC with serpentine fluid channel. The effects of phase change and temperature as well as two-phase flow and transport, electrochemical kinetics, and multicomponent transport on cell performance are accounted for simultaneously in this comprehensive model. The developed model was employed to simulate a single laboratory scale PEMFC with electrode area about 12 $cm^2$.

**Keywords:** proton exchange membrane fuel cell; numerical simulation; computation fluid dynamics

## 1. INTRODUCTION

A proton exchange membrane fuel cell has many prominent characteristics, especially short startup time under low temperature, which makes it become a promise power source for future transport tools (such as electrical vehicles). General speaking, PEMFCs as power sources of transport tools will often operate dynamically, for example during startup and stop, acceleration and deceleration of electrical vehicles. It is well known that good gas flow fields design and water balance is useful for the enhancement of fuel cell.

Hitherto, there have lots of numerical investigations on PEMFCs all over the world; however, most of them are based on stable and single phase mathematical model and are focused on single channel of simple cell structure such as straight channel [1-4]. Water management of PEMFC plays an important role for operation and performance optimization of PEMFC. Thus, many models focused on

water management. Bernardi et al. [2] developed a hydraulic model with assumptions that the membrane is fully hydrated with liquid water. However, this model is not suitable for a partially dry membrane. Yi et al. [5] developed one model for interdigitated flow fields considering liquid water. However the liquid water flow induced by capillary forces and gas flow induced drag was addressed by semi-heuristic equations. Natarajan et al. [6] developed a pseudo-three-dimensional model by extending their two-dimensional isothermal model. This model can be used to obtain qualitative insight into the distribution of liquid water in the backing layer. Two-phase flow modeling in the porous air cathode of a PEMFC was attempted by Wang et al. [7]. The transport coefficients in the stationary numerical two-phase model are parameterized as functions of the liquid water saturation. However, this model only considered the cathode half cell. Berning et al. [8] developed a 3D, two-phase PEMFC model based on computational fluid dynamics multiphase. Transport of liquid water inside the gas-diffusion layers is modeled using viscous forces and capillary pressure terms. Shimpalee et al. [9] developed a complete three-dimensional model, which treated the liquid water as component of the gas mixture. Steinkamp et al. [10] presented a 2D dynamic two-phase flow model accounting for all important transport processes in a PEM fuel cell. Unfortunately, the computational cost for simulation was quite high because of the high complexity of the model. Siegal et al. [11] presented a 2D model to account for the transport of liquid water in the electrode and treat all three forms of water as a separate phase and allow mass transport among them. Zhang et al. [12] developed a model including three forms of water: dissolved water in the electrolyte or membrane, and liquid water and water vapor in the void space. A one-dimensional analytic solution of liquid water transport across the CCL is derived from the fundamental transport equations [13]. Based on a dimensionless time constants analysis, it has been shown that liquid water production from the phase change process is negligible comparing to water production from the electrochemical process. In order to investigate the effect of flow fields structure on the cell performance, many researches focused on the some other flow fields design except the straight channel, such as serpentine channel and interdigitated channel [14-15], etc. Serpentine channel have been studied by many researchers both by experimental and numerical methods to know the distribution of temperature, pressure and species concentration in more detail [16-19]. The effect of the channel size on the cell performance of proton exchange membrane (PEM) fuel cells with serpentine flow fields was numerically investigated by a three-dimensional, two-phase model [16]. The local current densities in the PEM, oxygen mass flow rates and liquid water concentrations at the interface of the cathode gas diffusion layer and catalyst layer were analyzed to understand the channel size effect.

In this paper a three dimension model is employed to investigate a single cell PEMFC with serpentine flow fields, the distribution of some characteristic parameters as membrane surface temperature and some reference data for pressure loss and net water flux from anode to cathode are obtained for real design and operation of fuel cell.

## 2. DESCRIPTION OF MATHEMATICAL MODEL

The simplification assumptions considered in this model development are: 1) The flow in fuel cell is laminar everywhere. This is reasonable for the low velocity and low Reynolds number. 2) The

proton membrane is impermeable to gas species. 3) Isothermal boundary conditions are used for external wall and inlet stream. 4) The porous media such as diffusion layer and catalyst layer are isotropic and homogeneous, characterized by effective permeability and uniform porosity. 5) Water is generated in the catalyst layer in the form of vapor; condensation occurs after vapor partial pressure exceeds saturation vapor pressure.

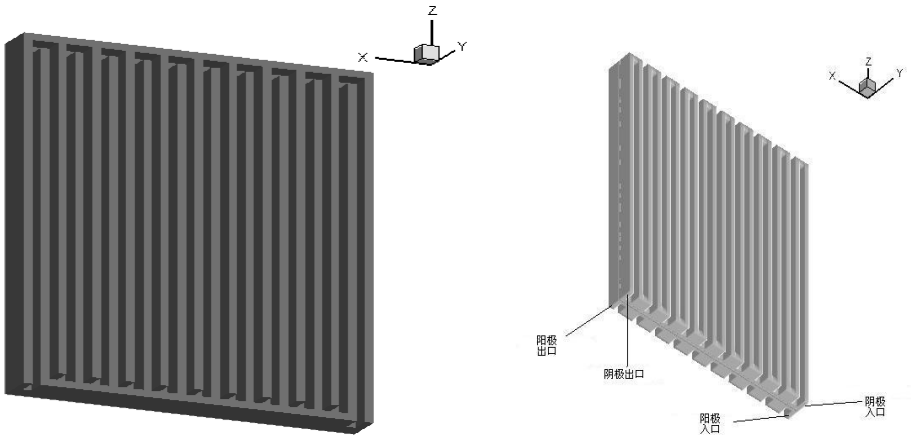


**A** **B**

**Figure 1.** Schematic of channel structure, components and grid partition of a single fuel cell; (a) Bipolar plate and channel structure (b)Components across membrane

*2.1 Governing Equation*

Numerical simulation is based on a three-dimension, multicomponent, non-isothermal and two-phase transportation model, which is a comprehensive model including mass, momentum, and energy and components transportation. The conservation equations appear the same form for the fluid channels, the diffusion layers, the catalyst layers and the membrane. So continuum equation, momentum equation, species conservation equation and energy conservation equation can be described as following respectively:

$$\nabla \cdot (\varepsilon \rho \boldsymbol{u}) = S_{\mathrm{m}} \tag{1}$$

$$\nabla \cdot (\varepsilon \rho \boldsymbol{u}\boldsymbol{u}) = -\varepsilon \nabla p + \nabla \cdot (\varepsilon \mu^{\mathrm{eff}} \nabla \boldsymbol{u}) + S_{\boldsymbol{u}} \tag{2}$$

$$\nabla \cdot (\varepsilon \rho \boldsymbol{u} C_i) = \nabla \cdot (-\rho D_i^{\mathrm{eff}} \nabla C_i) + S_i \tag{3}$$

$$\nabla \cdot (\rho \boldsymbol{u} C_p T) = \nabla \cdot (\lambda^{\mathrm{eff}} \nabla T) + S_T \tag{4}$$

Where $\varepsilon$ is porosity of porous media, $\rho$ is density of mixture, $\boldsymbol{u}$ stands intrisinic velocity of fluid, $S_{\mathrm{m}}$ is mass source term, $p$ is fluid pressure, $\mu^{\mathrm{eff}}$ is effective viscous coefficient, $S_{\boldsymbol{u}}$ is movement source term, $C_i$ is mass fraction of species $i$, $J_i$ is diffusion flux, $S_i$ is mass source term of species $i$, $T$ is

temperature, $C_p$ is isopressure heat capacity, $k^{\text{eff}}$ is effective heat conductivity, $S_T$ is energy source term. All the source term and corresponding calculation method can be found in literature [20].

### *2.2 Relation between Voltage and Current Density*

Considering voltage loss induced by ohm resistance and activation polarization, real operation voltage of a fuel cell can be explained as

$$V_{\text{cell}} = V_{\text{oc}} - \eta(x,y) - I(x,y)\cdot R_{\text{fc}} \tag{5}$$

Where $V_{\text{oc}}$ stands open circuit voltage, *I(x,y)* is local current density and $R_{fc}$ is electrical resistance including electrical resistance of proton and electron transportation, the local activation overpotential $\eta(x,y)$ is composed of two components: anode activation overpotential and cathode activation overpotential, the latter occupies main part, can be solved by following equation

$$\eta(x,y) = \frac{\mathrm{R}T(x,y)}{0.5F}\ln\left[\frac{I(x,y).p(x,y)}{I_{O_{O_2}}\, p_{O_2}(x,y)}\right] + \frac{\mathrm{R}T(x,y)}{1.0F}\ln\left[\frac{I(x,y).p(x,y)}{I_{O_{H_2}}\, p_{H_2}(x,y)}\right] \tag{6}$$

where F is Faraday constant, *T(x,y)*, *p(x,y)*, $p_{O_2}$ and $p_{H_2}$ is local temperature, pressure, oxygen partial pressure and hydrogen partial pressure. $I_{O_{O_2}}$ is cathode exchange current density, $I_{O_{H_2}}$ is anode exchange current density.

### *2.3 Boundary conditions*

Flow rate required for fuel and air can be solved by the following equation:

$$G_k = \theta\frac{I_{\text{avg}}A}{2\mathrm{F}}\frac{\mathrm{R}T}{pX_k} \tag{7}$$

where $A$ is operation area of cell, $X_k$ is mole fraction of species $k$ and $\theta$ is stoichiometry flow ratio.

Species concentration and temperature at the inlet is known, viz. first kind boundary; pressure outlet boundary is employed for the outlet, assuming pressure at the outlet as zero, and the other variables as temperature, species concentration and fluid velocity are set as fully developed. At interfaces of CL and membrane, Von Neumann boundary condition, i.e., zero fluxes is adopted as the membrane is impermeable to gas species. For the interface between fluid domain and solid domain, the flux of species is zero and velocity is no-slip, coupled boundary condition is applied for temperature. The temperature of external surface is considered in the fixed temperature way, i.e., the temperature on these surfaces equals to the cell temperature as 353.15K.

### *2.4 Numerical Procedure*

This model is implemented into the commercial CFD code Fluent 6.2, with custom developed user-subroutines that take account of the parameters and physicochemical processes associated with PEM fuel cells. The basic operation condition and some typical parameters are listed in table 1.

## 3. RESULTS AND DISCUSSION

Parameters of fuel cell dimension and base case used in this computation is listed in table 1. Other physics parameters can be obtained from Bernardi[1], or solved by method introduced in their literature.

**Table 1**. Physics parameters and base conditions

| Quantity | Value | Quantity | Value |
|---|---|---|---|
| Operating temperature /K | 353.15 | Pressure of anode inlet /kPa | $1\times101.3$ |
| Length of the channel /cm | 5.0 | Pressure of cathode inlet /kPa | $1\times101.3$ |
| Channel width /cm | 0.1 | Exchange current density of anode /A.m$^{-2}$ | 100 |
| Width of plate out channel /cm | 0.1 | Exchange current density of cathode /A.m$^{-2}$ | 1000 |
| Channel thickness /cm | 0.1 | Specific area of catalyst layer /m$^{-1}$ | $1.4\times10^{5}$ |
| Bipolar plate width /cm | 41*0.1 | Velocity at the anode inlet /m.s$^{-1}$ | 2.46 |
| Diffusion layer thickness /cm | 0.025 | Velocity at the cathode inlet /m.s$^{-1}$ | 13.15 |
| Catalyst layer thickness /cm | 0.0028 | Humidity of anode inlet stream | 80% |
| Membrane thickness /cm | 0.005 | Humidity of cathode inlet stream | 100% |
| Shoulder width /cm | 0.1 | Condensation rate /s$^{-1}$ | 1.0 |

### *3.1 Temperature distribution*

Figure 2 illustrates the temperature distribution on the membrane surface of cathode: (a) 0.6V, (b) 0.8V. It can be seen from the figure that the temperature decreases along the flow direction, the reason is the temperature increasing of membrane is mainly from heat source by joule heat, which is proportionally local current density. Simultaneously, the "channel effect" can be seen explicitly, that is the temperature under the channels is higher that under the shoulders, this can be explained from two aspects. On the one hand, the area under channel can get obtain fresh reactants more easily, so the reaction rates and local current density is larger than that under the shoulder; on the other hand, the flow velocity under the channel is higher than that under the shoulder, so the produced heat can be more easily removed by convectional heat transfer. Comparing (a) and (b), it can be found that the temperature decreases as the operation voltage increases, that is the current density decreases as the operation voltage increases, so the less heat will be produced. For the base case of voltage 0.6V, the temperature decreases from 357.55K around the inlet to 353.15K at the outlet, for the case of voltage 0.8V, the highest temperature is about 353.5K around the inlet. The obtained temperature distribution rule and "channel effect" is very similar to literature [17].

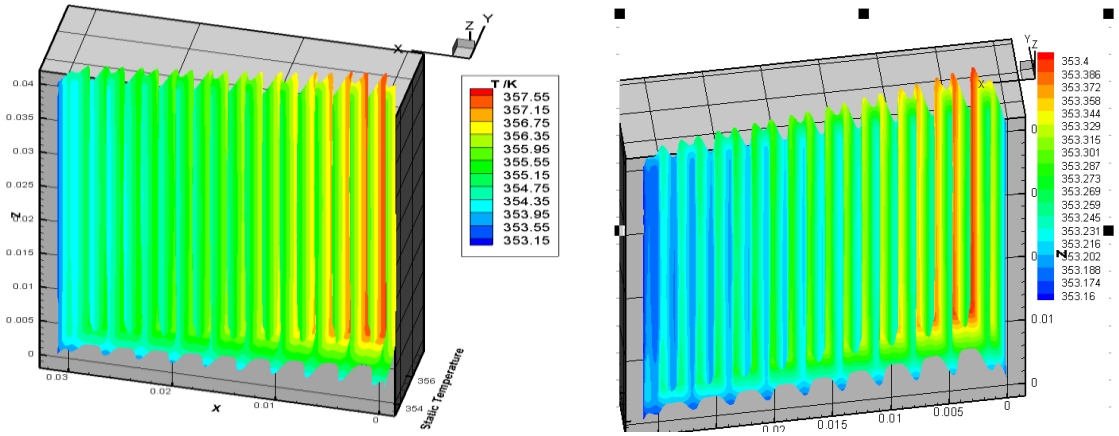


(a) 0.65V (b) 0.8V

**Figure 2.** The temperature distribution on the membrane surface of cathode with variation of voltage

*3.2 Effect of relative humidity of cathode inflow*

Table 2 lists the average net water flux coefficient for different voltage and relative humidity of cathode inflow, which response the net water flux per proton flux from the anode to the cathode and depends on the electroosmotic and reverse diffusion. It can be found from the table that the net flux coefficient doesn't change sharply under suitable voltage and RH, varies from 0.4 to 0.54. For the same RH, current density increases as the voltage decreases, the reverse diffusion decreases, this causes the increase of the net flux coefficient. For the same voltage, the net flux coefficient will increase at the inflow RH increase, which is because the increase of water vapor concentration of cathode will make the back diffusion increase.

**Table 2**. Net water flux per proton flux

| Voltage / RH | 0.4 | 0.5 | 0.6 | 0.7 | 0.8 |
|---|---|---|---|---|---|
| 0.6 | 0.3901 | 0.3987 | 0.4405 | 0.4904 | 0.5223 |
| 0.8 | 0.3978 | 0.4059 | 0.4468 | 0.4964 | 0.5278 |
| 1.0 | 0.4010 | 0.4085 | 0.4544 | 0.5037 | 0.5344 |

Table 3 and 4 lists the pressure loss (pressure difference between the inlet and outlet) of anode and cathode under different operation and relative humidity. It can be seen by comparing two tables that the pressure loss of cathode is higher than that of anode for the same case. Under the same operation voltage, the pressure loss of anode increases along with increase of RH; under the same RH, the pressure loss of anode will decrease at first, then increase and decrease at last as the operation voltage increase. Under the same operation voltage, the pressure loss of cathode will decrease firstly and then increases along with increase of RH for the low voltage, but the pressure loss of cathode will

increases along with increase of RH for the high voltage. Under the same RH, the pressure loss of cathode will increase as the operation voltage increase.

**Table 3.** Pressure loss of anode (Pa)

| Voltage / RH | 0.4 | 0.5 | 0.6 | 0.7 | 0.8 |
|---|---|---|---|---|---|
| 0.6 | 1289 | 1021 | 1172 | 1331 | 997 |
| 0.8 | 1323 | 1047 | 1195 | 1350 | 1009 |
| 1.0 | 1339 | 1056 | 1222 | 1372 | 1021 |

**Table 4**. Pressure loss of cathode (Pa)

| Voltage / RH | 0.4 | 0.5 | 0.6 | 0.7 | 0.8 |
|---|---|---|---|---|---|
| 0.6 | 4640 | 3672 | 3481 | 3283 | 2037 |
| 0.8 | 4543 | 3600 | 3416 | 3227 | 2005 |
| 1.0 | 5410 | 4683 | 3346 | 3167 | 1972 |

*3.3 Condensation rate*

Figure 5 illustrates the condensation rate for the different inflow RH of cathode with operation voltage 0.6V.

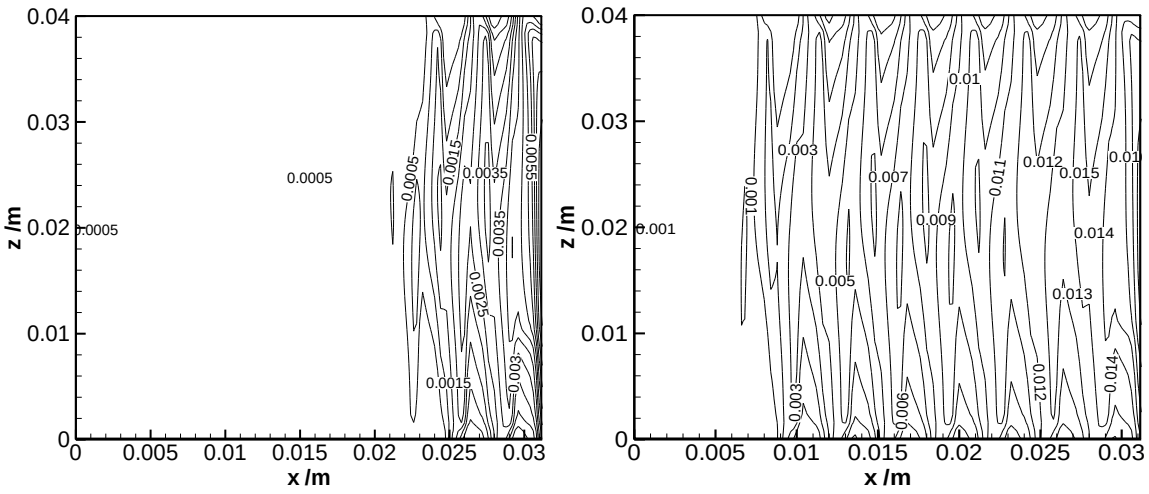


(a) 60% (b) 80%

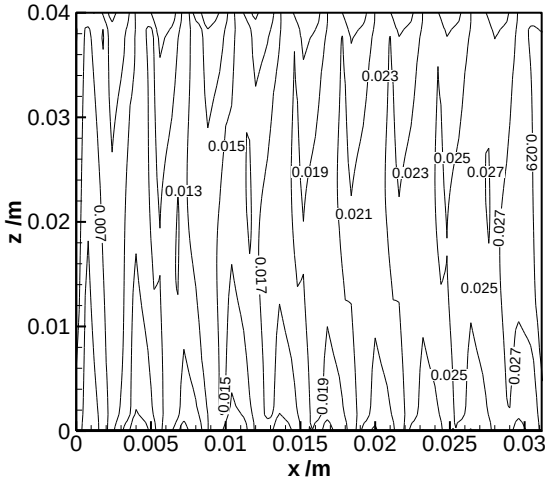


(c) 100%

**Figure 3.** Effect of cathode inflow RH on the condensation with operation voltage 0.6V

The same trends can be found that the condensation rate will increase along flow processes for the accumulation of water. When the RH is low, the front fluid can not be explicitly over-saturated, so the condensation rate is very low; when the RH is high, the condensation rate is large even around the inlet. Comparing condensation rate under different inflow RH of cathode, it shows that the higher RH, the higher condensation rate.

## 4. CONCLUSIONS

A three-dimension and two-phase mathematical model is developed to investigate characteristic parameters as temperature and condensation rate etc. variation with operation voltage and RH of cathode inflow. Computed results indicate that the temperature "channel effect" can be seen explicitly and the temperature decreases as the operation voltage increases; the condensation rate will increase along flow processes for the accumulation of water; the pressure loss of cathode is higher than that of anode for the same case; the net flux coefficient does not change sharply under suitable voltage and RH, varies from 0.4 to 0.54.

ACKNOWLEDGEMENTS
The research is supported by the National Natural Science Foundation of China (Grant Nos 11072220 and U1262109), the the Qianjiang Talents Plan of Zhejiang Province (Grant no. 2013R10069) and The Pre-research special foundation for interdisplinary subject at Zhejiang University of Science and Technology (No. 2011JC01Z)

## References

1. T. E. Springer, T. A. Zawodinski, and S. Gottesfeld, *J. Electrochem. Soc.*, 138 (1991)2334.
2. D. M. Bernardi and M. W. Verbrugge, *J. Electrochem. Soc.*, 139 (1992)2477.

3. Bonghwan Lee, Kiwon Park and Hyung-Man Kim，*Int. J. Electrochem. Sci.*, 8 (2013)219
4. Hannach M.， Prat M.， Pauchet J., *Int. J. Hydrogen Energy*, 37(2012)18996.
5. J. S. Yi and T. V. Nguyen, *J. Electrochem. Soc.*, 146 (1999)38.
6. D. Natarajan and T. V. Nguyen, *J. power sources*, 115 (2003)66.
7. Z. H. Wang, C. Y. Wang and K. S. Chen, *J. Power Sources*, 94 (2001)40.
8. T. Berning, D. M. Lu and N. Djilali, *J. Power Sources*, 106 (2002)284.
9. S. Shimpalee and S. Dutta, *Numerical Heat Transfer*, Part A, 8 (2003)111.
10. K. Steinkamp, J. O. Schumacher, F. Goldsmith, M. Ohlberger and C. Ziegler, *J Fuel Cell Science and Technology*, 5 (2008)011007.
11. N. P. Siegel, M. W. Ellis, D. J. Nelson and M. R. von Spakovsky, *J Power Sources*, 128 (2004)173.
12. X. Zhang, D. Song, Q. Wang, C. Huang, Z.-S. Liu, *J fuel cell science and technology*, 7 (2010)021009-1.
13. Prodip K. Das, Xianguo Li, and Zhong-Sheng Liu, in Engineering and Technology Conference FuelCell/2009, P. 85189, Proceedings of ASME 2009 Seventh International Fuel Cell Science, Newport Beach, California.
14. V. Thitakamol, A. Therdthianwong, S. Therdthianwong, *Int. J. of Hydrogen Energy*, 36(5) (2011) 3614.
15. L. Chen, H. Luan, Y. He, W. Tao, *Int. J. Thermal Sciences*, 51 (2012) 132.
16. X. Wang, W. Yan, Y. Duan, *Energy Conversion and Management*, 51 (2010) 959.
17. M. Wang, H. Guo, C. Ma, *J. Power Sources*, 157 (2006) 181.
18. F. Hashemi, S. Rowshanzamira, M. Rezakazemi, *Mathematical and Computer Modelling*, 55 (2012) 1540
19. J. M. Sierra, J. Moreira, P. J. Sebastian, *J. Power Sources*, 196 (2011) 5070.
20. G. Hu, J. Fan, *J. Power Sources*, 165 (1), (2007)171.